Surface & Coatings Technology 421 (2021) 127400

Contents lists available at ScienceDirect

Surface & Coatings Technology

journal homepage: www.elsevier.com/locate/surfcoat

Wear resistance and self-lubrication of electrodeposited Ni-SiC:MoS_2 mixed particles composite coatings

S. Pinate [a,*], P. Leisner [a], C. Zanella [a,b]

[a] Department of Materials and Manufacturing, School of Engineering, Jönköping University, Jönköping, Sweden
[b] Department of Industrial Engineering, University of Trento, Trento, Italy

ARTICLE INFO

Keywords:
Electroplating
Mixed dispersion coating
Nanocrystalline nickel
Microhardness
Wear
Self-lubrication

ABSTRACT

Ni-based mixed particles composite coatings were designed to achieve superior wear resistance by combining hard carbides and solid lubricants as a reinforcing particles mix. Pure nickel and single-particles composites were electrodeposited in the same conditions for benchmarking. A pre-study was carried out to optimise the current density to avoid loss of process efficiency due to hydrogen evolution. The production process was also improved by employing ultrasounds to avoid porosity and dendritic growth in the metal caused by conductive MoS_2 particles. The presence of MoS_2 particles led to nanocrystallinity in the nickel matrix, confirmed by electron backscatter diffraction (EBSD) maps and transmission electron microscopy (TEM). The microstructural changes and codeposition in the different composites were correlated to microhardness and pin-on-disc tests. An extremely high hardness was observed in the mixed particles composite (≈1110 HV) due to the combined effect of the nanocrystalline matrix and high codeposition rate (≈15 vol% SiC and ≈8 vol% MoS_2). The codeposition of MoS_2 particles provided a self-lubrication capability to the coating, reducing the friction coefficient compared to pure Ni from 0.15 to 0.07. The wear rate was reduced more than 12 times by the mixed reinforcement compared to pure Ni and more than 6 times compared to Ni-SiC.

1. Introduction

The improvement of wear resistance in composite materials provided by a second phase has been a significant area of interest in the last decades [1–4]. The process of electrodepositing coatings can be adjusted to produce composites with hard particles, e.g. SiC, Al_2O_3, WC, strengthening the material depending on their incorporation rate [5–7], dispersion within the matrix [8,9], and effect as grain refiner of the metal microstructure [10–13]. Likewise, self-lubricating particles, e.g. polytetrafluoroethylene (PTFE), graphite, and MoS_2, are selected to reduce wear by providing the composite coating with a self-lubrication capability to reduce friction [14–16].

Many studies successfully proved that nanosized carbides increase wear resistance in Ni-based composite coatings. Lanzutti et al. [17] hardened Ni deposits by nano-SiC (ΔHV ≈ 100), halving the wear rate of the material. Gül et al. [18] and Zhou et al. [19] also reported that the addition of nano-SiC in the metal increased hardness, and thus decreasing the wear rate. On the other hand, other studies pursue the reduction of wear by decreasing the friction by adding self-lubricant particles. He et al. [14] reported that the addition of WS_2 in the composite coating ensured a low coefficient of friction (0.17–0.2) compared to NiP (0.5). Cardinal et al. [15] reported self-lubrication by MoS_2, which almost halved the friction coefficient compared to Ni—W from 0.27 to 0.14, in agreement with the findings reported by He et al. [16], where NiP friction coefficient was reduced from ≈0.4 to ≈0.05 by 7.9 wt% MoS_2 entrapment.

Most studies focus on achieving high wear resistance by designing composites with a single type of particles. Only recently, attention has been brought to the future potential of multifunctional composite coatings [20], for instance, one designed with combined functionalities: hardening and self-lubrication. Pinate et al. [21] reported an improvement in the wear resistance of pure nickel by mixed nanoSiC:Graphite dispersion, reducing wear rate around 30%. Huang et al. [22] successfully produced NiP microSiC:PTFE mixed particles composites by electroless, reporting a better wear resistance when both particles were combined, reducing wear rate from 2.52 (10^{-6} mm^3 N^{-1} m^{-1}) in the pure metal to 0.36 (10^{-6} mm^3 N^{-1} m^{-1}) in the mixed particles composite. Likewise, Tang et al. [23] designed a Ni Al_2O_3:PTFE mixed dispersion coating to improve wear resistance, reporting a preferable low friction and anti-wear behaviour in the mixed reinforcement

* Corresponding author.
E-mail addresses: santiago.pinate@ju.se (S. Pinate), peter.leisner@ju.se (P. Leisner), caterina.zanella@ju.se (C. Zanella).

https://doi.org/10.1016/j.surfcoat.2021.127400
Received 21 April 2021; Received in revised form 27 May 2021; Accepted 3 June 2021
Available online 15 June 2021

composite. Zhou et al. [24] studied superhydrophobic coatings fabricated by the codeposition of nanosized WS_2 and WC particles in Ni. Similar to the mentioned studies, significant abrasive resistance was observed in the mixed particles composite, holding the superhydrophobicity for 2.5 times the distance (>10,000 mm) compared to the single-particle composite.

The present work aims to design and produce superior wear resistance nickel composite coatings by adding SiC 60 nm and MoS_2 90 nm as a dispersion mix in a 1:1 g L^{-1} ratio. Composites containing single particles were also produced to show the advantages of composites design with mixed dispersion. The composite coatings were produced by electrodeposition from an additive-free nickel Watt's bath [25]. The codeposition effect on the microstructure was studied by electron backscatter diffraction (EBSD) maps and transmission electron microscopy (TEM). All the deposition parameters were maintained constant to relate any modification in the matrix solely to the particles codeposition, thereby defining a relationship between electrocodeposition, microstructure, and coatings performance in term of hardness and wear resistance. Therefore, the electrodeposition bath chemistry was additive-free to avoid affecting the metal microstructure by the presence of additives [26–29].

A pre-study was carried out in the Ni-MoS_2 and Ni-Mix composites to optimise their production, comparing two agitation modes: stirring by a rotating magnet and ultrasonic (US) agitation. The two agitation modes were compared in terms of coating quality. Particle agglomeration is generally to be avoided and becomes notably harmful for the electrodeposition of metal in the presence of conductive particles [30,31]. US agitation breaks particle agglomerates [9] and improves their dispersion if applied during electrodeposition. During the pre-study cathodic polarisation curves were also monitored to define the optimal current density parameter to produce Ni-Mix composites without major losses of current efficiency due to hydrogen evolution catalysed by MoS_2 particles [32].

2. Experimental and characterisation details

2.1. Preparation of specimens

The electrodeposition was carried out with the parameters reported in Table I, in a thermally controlled cell at 45 °C with a volume of 500 mL with the electrodes arranged vertically with a distance of 7 cm. The deposits were produced from an additive-free Watt's bath [25] as reported in Table I and with a powder load of 10 g L^{-1} of SiC nano-size powder (Iolitec GmbH #NC-0002 spherical β-SiC 60 nm) or nano-MoS_2 (Iolitec GmbH #NC-0017 spherical MoS_2 90 nm). Mixed particles composites were produced from a dispersion mix of SiC and MoS_2 with a ratio of 10:10 g L^{-1}.

Before plating, the substrate (low carbon steel plates, 3 cm × 5 cm) was mechanically ground with SiC grade #1000, cleaned ultrasonically in an alkaline soap and activated by pickling for 8 min in 2.5 M H_2SO_4. The pH of the electrodeposition bath was set to 3.0 and controlled during the process using sulfuric acid or sodium hydroxide.

Three samples were produced for each condition under agitation by an ultrasonic (US) horn (24 kHz, 0.087 W cm^{-3}) immersed in the cell and placed 6.5 cm away from the electrodes. Pure nickel, Ni-SiC and Ni-MoS_2 were produced by a direct current (DC) at 4 A dm^{-2} while Ni-Mix were deposited under DC at 2.33 A dm^{-2}. The current density of Ni-Mix was optimised as the result of a pre-study, as reported in Section 3.1. The total deposition time in Ni-Mix was increased to maintain the same charge.

The pre-study was carried out by producing Ni-MoS_2, and Ni-Mix composites with the same parameters reported in Table I, except that both composites were produced using a direct current (DC) at 4 A dm^{-2} and under stirring by a rotating (200 rpm) cylindrical magnet (polymer coated, 0.7 cm diameter and 6 cm in length) centrally located at the bottom of the cell. The electrodes were 1.5 cm away from the magnetic stirrer.

The bath suspension was continuously stirred by a rotating magnet before electroplating to avoid agglomeration of particles and turned off during the deposition when the US was applied. The samples were ultrasonically washed for 1 min in water after plating to remove any loose particles from the surface.

The current efficiency (CE) of the process was obtained by comparing the theoretical deposited mass calculated by Faraday's law to the weight of the deposited mass minus the particles' mass, considering the molar mass of Ni (58.69 g mol^{-1}) and its density (8.91 g cm^{-3}).

Table I
Electroplating bath composition and parameters.

$NiSO_4{\cdot}7H_2O$	240 g L^{-1}	Particles concentration	Single: 10 g L^{-1}; Mix: 10:10 g L^{-1}
$NiCl_2{\cdot}6H_2O$	45 g L^{-1}	SiC particles size	60 nm
H_3BO_3	30 g L^{-1}	MoS_2 particles size	90 nm
pH	3.0	Agitation	US; 24 kHz, 0.087 W cm^{-3}
Temperature	45 °C	Current density	DC; 4 A dm^{-2} and 2.33 A dm^{-2}
Anode	Ni sheet; 99.9% purity	Total deposition time	30 min and 52 min
		Coating thickness	≈ 24.5 μm

2.2. Polarisation test

Potentiodynamic cathodic polarisation curves were measured in the same conditions as the electrodeposition bath (Table I) containing the dispersion powder mix SiC:MoS_2 while agitated by US oscillation or silent. The polarisation was applied from OCP to cathodic polarisation equivalent to a current density of 4.5 A dm^{-2}. An Ag/AgCl (3 M KCl) was used as the reference electrode, and the counter and working electrode were the same materials as the anode and substrate used in the electrodeposition. The distance between the reference and working electrode was approximately 1 cm. An IVIUM Vertex potentiostat was employed for the electrochemical measurements with a potential step of 1 mV and a sweep rate of 10 mV s^{-1}. The ohmic potential drop (IR) was not compensated, considering the high conductivity of concentrated Watts electrolytes.

2.3. Characterization of specimens

The coatings' surface and the cross-section were analysed by scanning electron microscopy (SEM, JEOL 7001F and TESCAN Lyra 3). The samples were also prepared for cross-sectional scanning transmission electron microscopy (STEM) by conventional mechanical polishing and Ar-ion milling methods. STEM was carried out using a Tecnai G2 TF20 UT electron microscope, operated at 200 kV. Images were acquired in STEM mode using a high-angle annular dark-field (HAADF) detector.

The coatings were analysed by electron backscattered diffraction (EBSD, EDAX-TSL) in cross-section after mechanical polishing with a final step of 0.5 μm particles suspension. The measurements were performed with an electron probe current of 4.46 nA at an acceleration voltage of 15 kV, and the map was built with a step size of 80 nm. The EBSD maps were analysed by OIM 5™ software in the growth direction (perpendicular to the cross-section) on two samples for each plating condition. A grain was defined as a region consisting of at least three similarly oriented connected points with a misorientation <10°. The grain size was calculated by the number of data points contained in this region, disregarding all the data points with coefficient index (CI) <0.1. Twin boundaries were excluded from the calculations. The average grain area was calculated by weighting the value of the area fraction of each grain, and the grain diameter was extrapolated by considering the grain as a circle.

The composition and quantification of SiC and MoS_2 particles was by wavelength dispersive X-ray spectroscopy (WDS, EDAX-TSL) for a better

resolution of light elements. The weight % of Si and Mo was quantified based on pure Si and Mo standards, respectively. The analysis of the standard and each specimen was performed using an acceleration voltage of 10 kV and beam current ranging from 15.5 nA to 18.3 nA. The volume content of silicon carbide was calculated starting from Si data and the molybdenum disulfide content starting from Mo data, and considering both powders to be stochiometric. Both particles contents were expressed as the average value of five different WDS area measurements of two different specimens.

The microhardness and the reduced elastic modulus (E_r) of the deposits were obtained from load-displacement curves by micro-indentation with a Berkovich pyramidal-shaped diamond tip (NanoTestTM Vantage). The measurements were done on the cross-section with an indentation load of 100 mN and a dwell time of 10 s. Fifteen repetitions were done on two samples for each condition, and the values were expressed as the average and standard deviation.

The tribological tests were performed in dry condition using a pin-on-disk test (NanoTestTM Vantage) with a load of 1 N and a sliding distance of 1.32 m. The coated samples were rotated at 70 RPM against a diamond ball (diameter 100 μm), acting as counter material. The friction coefficient was recorded continuously and automatically during the wear tests by a friction probe connected to the tip.

The wear track morphologies were analysed by a surface profilometer (Surtronic® S-100 Taylor Hobson®) and scanning electron microscope (SEM). The volumetric wear factor ($mm^3\ Nm^{-1}$) was calculated by dividing the worn volume (mm^3) excavated by the counter material, determined by profilometry measured from the surface of the sample, by the applied load (N) and the total sliding distance (m). The surface roughness was measured by a surface profilometer (Surtronic® S-100 Taylor Hobson®), and R_a was expressed as the average value of eight different measurements with 1 mm length.

3. Results and discussion

3.1. Pre-study results

The scanning electron microscopy (SEM) imaging in cross-section (Fig. 1a) for Ni-MoS_2, revealed extensive porosities and irregular surface topography, while in Ni-Mix, large cavities extending from the surface to the substrate were also visible (Fig. 1b). Previous studies reported similar defects in Ni-based composites with MoS_2 particles [15,30,31]. The catalytic effect over the hydrogen reduction by the MoS_2 particles caused intense hydrogen evolution [32], leading to porosity due to H_2 bubbling. Furthermore, the flake-shaped MoS_2 particles or agglomerates, once anchored in the metal, caused changes in the current distribution at the cathode surface, causing an uneven nickel electrocrystallisation, which led to dendritic structures and voids between the growing structure. To decrease the negative impact in the electrocrystallisation by conductive particles, Zhou et al. [30] improved the dispersion of MoS_2 particles by high-shear mixing, significantly improving the quality of nickel deposition. In the present study, agitation by an ultrasonic (US) horn during electrodeposition was chosen, instead of stirring, based on its capability to reduce agglomeration [9,33] and improve the dispersion of electrically conductive particles [34,35].

The US applied during the electrodeposition modified the current efficiency (CE) of the process compared to stirring by a magnetic rotator. Under stirring, the CE of Ni-MoS_2 was around ≈70%, comparable to the values observed by Chang et al. [36], where a CE (≈70%) was reported under similar electroplating parameters (4 A dm^{-2}, pH 4 and stirring). The CE of Ni-MoS_2 under US agitation slightly dropped to about ≈65%, thereby not requiring further optimisation. However, when stirring was substituted by US agitation in Ni-Mix deposition, a significant drop in CE to approximately ≈33% was observed under the US, compared to the ≈81% CE observed under stirring. The decrease in CE under US agitation was due to an increase in hydrogen evolution [37], observed by pH changes measured before and after electrodeposition. While in Ni-MoS_2 the ΔpH was about ≈0.4, Ni-Mix showed a considerable increase ΔpH ≈ 0.8.

A potentiodynamic cathodic polarisation was used to analyse the changes in the reduction reaction. Fig. 2 shows the cathodic polarisation curve for Ni-Mix deposition at the cathode under silent (Coloured dark blue) and US agitation (Coloured light blue).

The Ni-Mix silent process exhibited a curve with a steeper slope in contrast to the process under US agitation. Ni-Mix under silent agitation and at the process current density (4 A dm^{-2}) reported a lower potential (≈1.46 V vs reference) compared to Ni-Mix under US (≈2.03 V vs reference). Therefore, under US agitation, Ni-Mix required a higher potential to reach the same current density as in silent agitation (4 A dm^{-2}). Electrochemical reactions under a high overpotential at acidic pH support higher hydrogen evolution reaction rates, reducing the current efficiency. Consequently, the Ni-Mix silent process reported a better CE (≈81%) at the process current density (4 A dm^{-2}) compared to Ni-Mix under US (≈33%).

In order to optimise the process, Ni-Mix under US agitation was electrodeposited under a new current density (2.33 A dm^{-2}), matching the Ni-Mix silent cell potential (≈1.46 V vs reference). The CE of the process under the new current density (Fig. 2, red-coloured dotted line) was increased to 78%. Hereinafter, Ni-Mix will refer to the composites electrodeposited under the new current density, while the rest of the

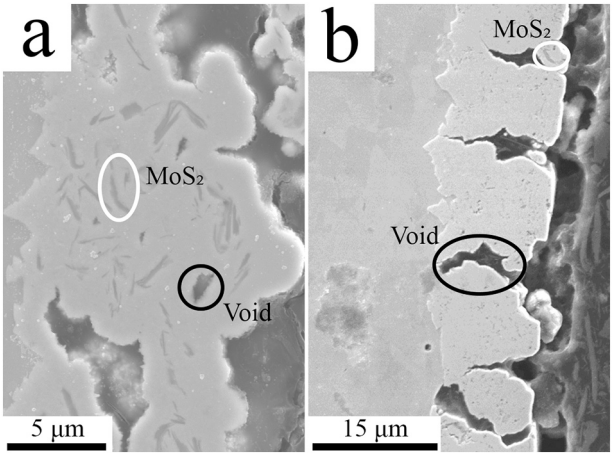

Fig. 1. SEM cross-section image of composites produced under stirring. (a) Ni-MoS_2/DC4 (b) Ni-Mix/DC4. MoS_2 particles are indicated by white-coloured ovals represent, and voids by the black-coloured.

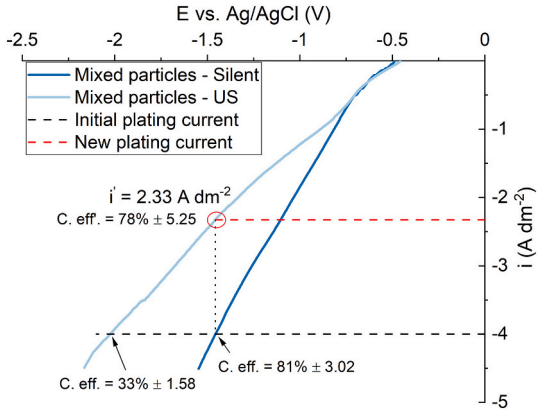

Fig. 2. Cathodic polarisation curves for the electrodeposition of Ni-Mix composite SiC:MoS_2 under US and silent agitation, with a Watts electrolyte (Table I).

samples were electroplated at 4 A dm^{-2}.

An experimental analysis employing changes in the US agitation or different MoS_2 particles concentration was outside the scope of the pre-study. However, future studies should focus on the effect of variations in the US power and probe placement on the kinetics of nucleation and diffusion-controlled growth of nickel deposits in the presence of MoS_2. Ultrasonic agitation may well significantly affect mass transport, thus modifying also the limiting current of the electrodeposition process, as described by Coleman et al. [38].

3.2. Coatings electrodeposition

Particles were added into the nickel electrolyte after the bath was set at pH 3.0. SiC addition had a negligible effect on the pH, raising the value to 3.06, while MoS_2 particles lowered the pH to 2.52. When added as a mixed dispersion, the pH decreased to 2.77. The acidification of the electrolyte after MoS_2 addition was also reported by Chang et al. [36]. Before electrodeposition, pH was adjusted to 3.0.

The electrodeposition of pure Ni using US agitation showed a minimal pH variation ($\Delta pH \approx 0.05$), while in Ni-SiC with US, the increase was around ≈0.1. In both cases, the current efficiency (CE) of the process was around 95%. Therefore, confirming that the increase in pH and loss of process efficiency was due to MoS_2 particles.

Fig. 3 shows cross-sectional SEM observation of the deposits, and Table II the particles codeposition rates. US agitation promoted a good particle dispersion in Ni-SiC(US). Particles were observable across the deposit (Fig. 3a), both as finely disperse individual particles or as small-sized agglomerates (<500 nm) as observed by the inlet SEM image in high magnification. SiC codeposition rate (≈7.6 vol%) was relatively high compared to other studies with nano-SiC [6,39–41]. US agitation promoted particle transport toward the cathode, allowing a better entrapment by the growing metal [9,33,35]. Besides, promoting particle dispersion. Furthermore, the benefits of agitation by US as an alternative to stirring by a rotating magnet are evident when comparing the SiC content (Table II) to previous studies carried out by the authors under the same electrodeposition set-up varying only the agitation mode. The codeposition of SiC under stirring was significantly lower (≈1.6 vol% [21]) with the same powder load as in this study (10 g L^{-1}), and despite doubling the powder load (20 g L^{-1}), the content was still lower (≈4.5 vol% [42]), showing the capacity of US agitation in producing rich nanocomposite deposits.

Fig. 3b shows the Ni-MoS_2(US) deposit under US agitation. The use of US decreased the number of porosities and their dimension compared to the ones under stirring (Fig. 1a). Moreover, Ni-MoS_2(US) deposits had also the same appearance as Ni-MoS_2 composites produced under high-shear mixing [30], showing a correlation between the two methods. Furthermore, MoS_2 content was also comparable, ≈12 wt% compared to 8.7 wt% [30]. The cross-section SEM image also shows a broad particle-size distribution with MoS_2 particles ranging from micrometre size to around 500 nm, as observed under high magnification, different from the reported nominal particles size. Zhou et al. [30] also reported broad particle-size distribution, reduced by high-shear mixing.

Fig. 3c shows a clear particles dispersion and codeposition, evidencing a strong synergistic effect between powders. Ni-Mix(US) composites showed an increased in SiC content, up to 14.9 vol%, almost doubling the codeposition rate observed in the single Ni-SiC composite (7.6 vol%), while MoS_2 content decreased, down to 8.3 vol %, contrasting the high content (19.6 vol%) observed in Ni-MoS_2.

As particles mixture, SiC was finely dispersed as small agglomerates populating the whole deposit homogeneously. The particle size of the codeposited MoS_2 as a mixed dispersion was smaller compared to the ones codeposited in Ni-MoS_2(US). Jiang et al. [43] observed PTFE particles covered by nano-SiC after codepositing mixed nano-SiC:PTFE in a nickel matrix. A similar interaction between MoS_2-SiC might have caused a larger codeposition of SiC per MoS_2 particle. MoS_2 particles, larger than the SiC particles, might have attracted nano-SiC in their

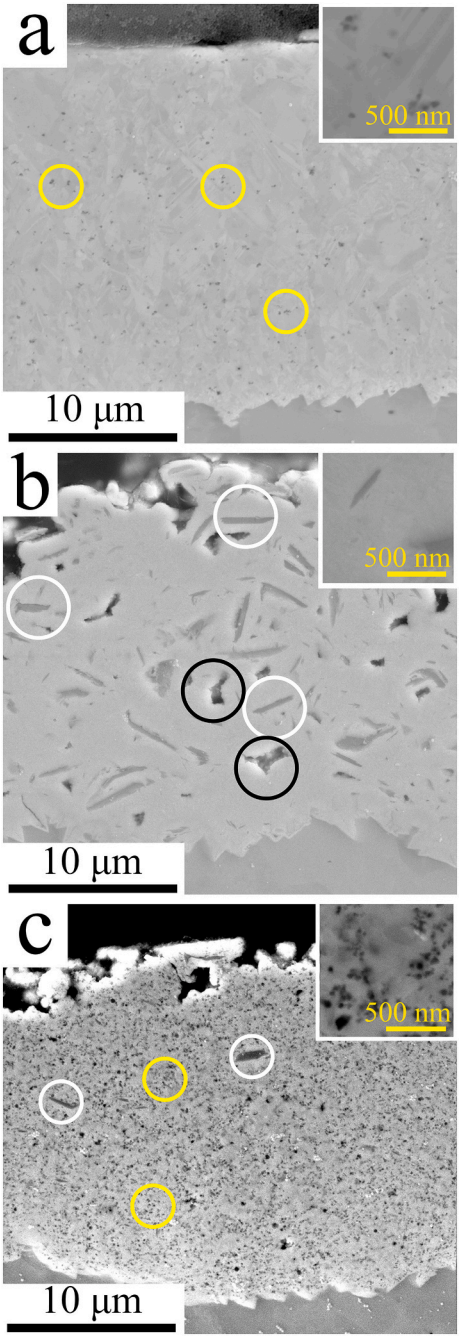

Fig. 3. SEM cross-section image of composites produced using US agitation. (a) Ni-SiC/DC4 (b) Ni-MoS_2/DC4 (c) Ni-Mix/DC2.3. The insets show high magnification images of the particles. Some of the SiC particles are encircled in yellow, MoS_2 particles in white and porosity in black.

Table II
Codeposited SiC and MoS_2 weight and volume content (%) under US agitation as determined by WDS.

	SiC (US)	MoS_2 (US)	Mix (US)	
			SiC	MoS_2
Vol%	7.64 ± 1.25	19.55 ± 1.60	14.85 ± 1.10	8.27 ± 0.53
Wt%	2.91 ± 0.50	12.21 ± 1.11	5.86 ± 0.69	5.41 ± 0.30

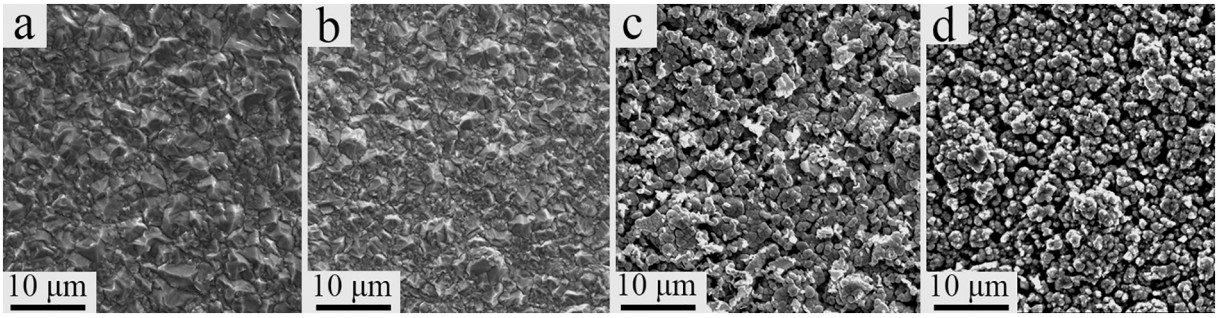

Fig. 4. SEM surface topography. (a) Pure Ni (DC4/US) (b) Ni-SiC (DC4/US) (c) Ni-MoS_2 (DC4/US) (d) Ni-Mix (DC2.3/US).

Table III
Average grain area (GA - µm^2) and arithmetical mean roughness (R_a - µm).

	Ni (US)	Ni-SiC (US)	Ni-MoS_2 (US)	Ni-Mix (US)
Grain area (µm^2)	7.21 ± 0.27	4.24 ± 0.30	< 0.02	< 0.02
Roughness (R_a - µm)	0.27 ± 0.04	0.32 ± 0.07	0.74 ± 0.11	0.73 ± 0.06

surroundings, promoting SiC codeposition and a selective entrapment of MoS_2, allowing only the smaller particles to codeposit. Ni-Mix deposits did not show any porosity problems reported in the Ni-Mix using stirring (Fig. 1b).

3.3. Surface morphology and microstructure

The surface topography of the pure Ni and Ni-SiC sample was pyramidal-shaped (Fig. 4a and b), showing comparable roughness values (Table III). Garcia-Lecina et al. [44] and Tudela et al. [45] also reported similar structures in electroplated nickel from additive-free Watts under US agitation. The composites containing MoS_2 particles had an irregular topography with protruding structures distributed across the surface (Fig. 4c and d). These differences might be due to the preferential reduction of Ni ions over the MoS_2 particles. Similar structures were described in previous studies with MoS_2 particles in Ni with no US agitation [30,31]. Furthermore, these structures were also observed in NiP-MoS_2 composites [16,46], where the addition of MoS_2 particles effectively modified the surface topography from smooth to rougher surfaces. He et al. [14] reported similar surface topographies as well in NiP after the addition of WS_2, exposing the strong influence that conductive particles such as MoS_2 and WS_2 have in the local current distribution during the electrodeposition of metal and their growth kinetics. Although MoS_2 content was higher in Ni-MoS_2 than Ni-Mix (Table II), the resulting surface roughness was similar (Table III).

The average grain areas (GA) were calculated from the EBSD maps (Fig. 5) and are reported in Table III. The values of Ni-MoS_2 and Ni-Mix are reported as 'lower than' (<) since the grain size was below the technique resolution, confirmed as nanocrystalline microstructures by transmission electron microscopy (TEM) imaging (Fig. 6). The smaller grains, undetected due to the resolution limit, remained unindexed and unable to be included in the grain area calculation. Hence, the grain area value of Ni-MoS_2 and Ni-Mix and was supposed to be lower than the

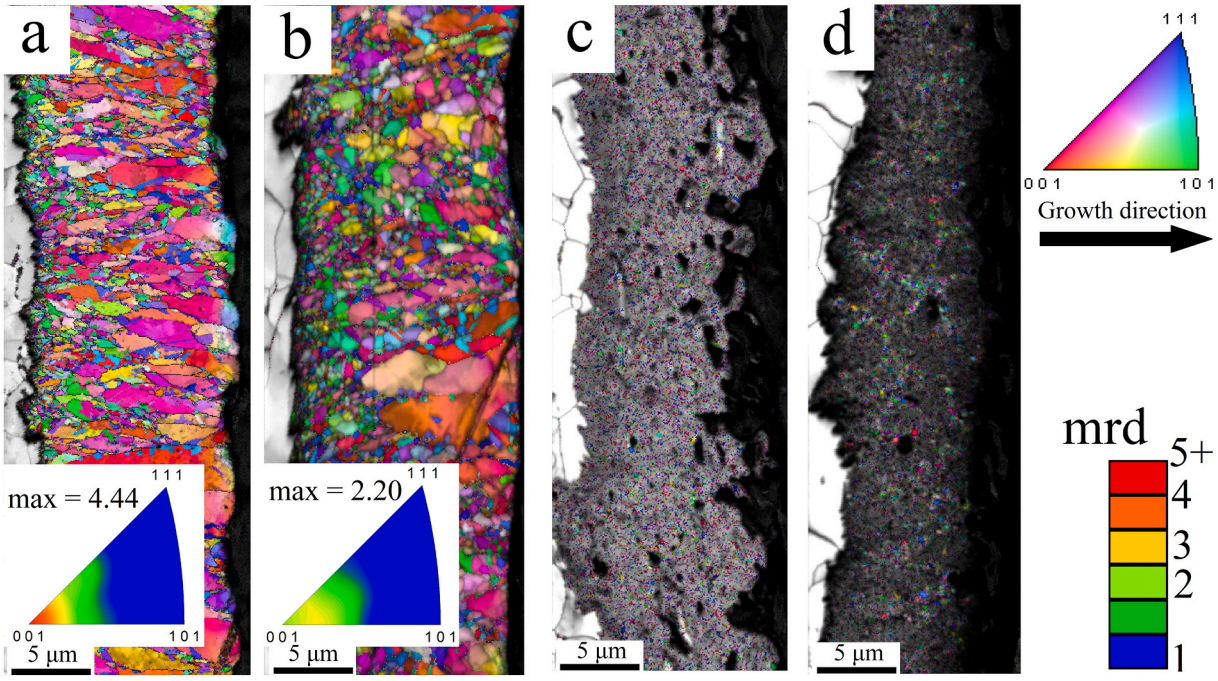

Fig. 5. Orientation map, colour-coded in relation to the electrodeposits' growth direction, shown by an arrow in the figure, and the equivalent inverse polar figure, including the max texture intensity in units of multiples of random distribution (mrd) as indicated by the colour bar. (a) Pure Ni (DC4/US) (b) Ni-SiC (DC4/US) (c) Ni-MoS_2 (DC4/US) (d) Ni-Mix (DC2.3/US).

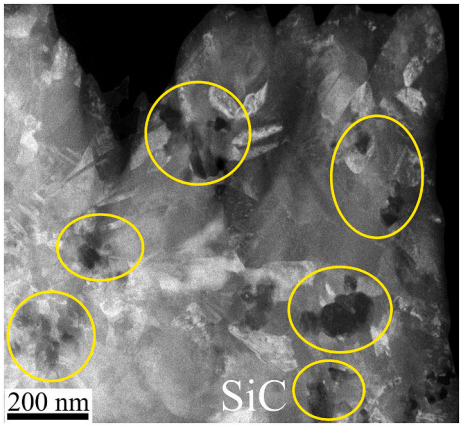

Fig. 6. TEM cross-section image of Ni-Mix/DC2.3 produced under US agitation. SiC particles agglomerates are indicated by the yellow-coloured ovals.

calculated.

Fig. 5 shows the complete change from columnar growth in pure Ni (US) (Fig. 5a) to smaller, equiaxial-like growth in Ni-SiC(US) (Fig. 5b). SiC codeposition caused grain refinement in the deposit, reducing the grain area considerably compared to pure Ni(US) (Table III). Well-dispersed by the US, numerous SiC particles promoted nucleation and growth of smaller grains. The observed grain refinement caused by SiC addition was in agreement with previous studies [6,41,47].

He et al. illustrated the mechanisms of growth of NiP with the addition of WS_2 [14] and MoS_2 [16], the conductive particles piled over the cathode surface, promoting an irregular cathodic surface. Once at the cathode, the conductive particles changed the electric field, leading to a higher current density on their surface. The nucleation of Ni ions would be preferred on the surface particles instead of on the surrounding area. The effect described by He et al. was observed in Ni-MoS_2(US) (Fig. 5c) and Ni-Mix(US) (Fig. 5d), multiplied by the high number of MoS_2 particles, promoted by the US, and thus provoking the growth of a nanocrystalline microstructure even without additives (Fig. 6). The nanocrystallinity in Ni-MoS_2 composites was also reported by Shourije et al. [48], although the authors linked the presence of saccharine to the resulting structure. Tudela et al. [34] used an additive-free bath to deposit Ni-WS2 coatings with a similar nanocrystalline structure as the ones seen in this study. Garcia-Lecina et al. [35] also described marked grain refinement of the Ni microstructure when WS_2 particles were included, pointing out the possible role of the electrical conductivity of WS_2 particles in the microstructure.

The inverse pole figures corresponding to the EBSD maps in cross-section are reported in Fig. 5. Ni-MoS_2(US) and Ni-Mix(US) nanostructures did not allow the EBSD mapping to provide enough data to build accurate polar inverse figures. Therefore, these were not included in Fig. 5. Pure Ni(US) and Ni-SiC(US) inverse polar figures showed a ⟨100⟩ preferential growth direction. This growth direction was related to the so-called 'free mode' nickel crystal uninhibited growth [37]. The ⟨100⟩ crystal orientation was dominant in the pure Ni samples, leading to a textured microstructure (Fig. 5a). The presence of SiC nano-particles promoted an inhibited growth in nickel [5,6,41], reducing the max intensity of the textured microstructure (Fig. 5b). The grain refinement prompted by the particles led to an increase in smaller, more randomly oriented grains instead of larger columns, commonly seen in a textured <100> growth. Moreover, hydrogen evolution observed by the change in pH also contributed to reducing the preferential crystal growth orientation. H_{ads} and H_2 are known inhibitors of the Ni growth [37], and the local alkalisation during electroplating, because of H^+ reduction, might have also favoured the formation of nickel hydroxide, a strong growth inhibitor [37].

3.4. Mechanical properties

The microhardness tests showed an increase in hardness linked to the combined effect of grain size and dispersion hardening. Grain refinement was promoted by particle codeposition, i.e. increasing the number of boundaries, leading to a reinforcement of the metal by grain size strengthening. Since MoS_2 is softer than Ni, additional particle strengthening was possible only in the composites with SiC particles.

The hardness of electroplated pure Ni(US) showed values of about 270 HV (± 28.41), in agreement with the reported results from previous studies under similar parameters [33,44,45]. Ni-SiC(US) deposits showed hardness values up to 448 HV (± 35.27) due to the well dispersed and high content of nanoparticles and the resulting grain refinement. Gyawali et al. [49] reported similar Vickers microhardness (≈500 HV) in additive-modified electroplated Ni-SiC (270 nm) composites. Other studies [17,40–42] also described hardening linked to the combination of codeposition and grain refinement under silent agitation.

The impact of the grain refinement effect caused by conductive particles was noticeable in Ni-MoS_2(US). The resulting nanocrystalline microstructure showed hardness values (446 HV ± 112.48) as high as Ni-SiC(US), despite MoS_2 particles are softer than Ni or SiC. Therefore, Ni-MoS2(US) hardness must be attributed to the numerous grain boundaries hindering dislocation mobility. The high scattering in hardness values might be due to the porosity and the soft MoS_2 particles. Previous studies [15,30,48] reported a decrease in hardness in Ni after MoS_2 codeposition.

Due to the combined effect of nanocrystallinity, i.e. grain size strengthening and particle hardening given by the high nano-SiC content (≈15 vol%), Ni-Mix composite held the highest microhardness, up to 1110 HV (± 200.49). To the best of the authors' knowledge, these hardness values have not been reported before in additive-free electroplated nickel-based composites.

Pure Ni(US) (170.45 ± 5.86 GPA) showed similar Young's modulus (Table IV) to the one reported in a previous study of electrodeposited nickel at 2 A dm^{-2} (165 GPa) [50]. The addition of nanoparticles increased the reduced Young's modulus (E_r) of nickel. This result was expected considering the composites' rule of mixture [51] and considering the elastic modulus values reported by Magnani et al. [52] for β-SiC (427 ± 2 GPa) and MoS_2 by Li et al. [53] (265 ± 13 GPa). The addition of a stiffer second phase increased the E_r value, leading to lower elasticity in all composites.

3.5. Tribological study

The average friction coefficients (COF) are reported in Fig. 7, along with the volumetric wear factor for all samples. The decrease in worn volume was evidently connected to the particles addition and hardness increase, showing the established [1,3,54] indirect relationship between high hardness and low wear, in addition to self-lubrication capability. The friction coefficient is dependent on both the adhesive and deformation force [55]. Ductile materials would be prone to adhesive wear leading to material detachment, while high friction, i.e. the material surface resisting the motion force, would lead to ploughing and pile-up [56]. These physical events would result in debris left in the wear track after the passing counter material like those observed in Fig. 8a and b.

The codeposition of nano-SiC increased the COF compared to pure Ni from ≈0.15 to ≈0.37, in agreement with the results presented by Gyftou et al. [40]. However, in contrast to other studies [17,19,57] where a decrease in COF in Ni-SiC composites was reported, compared to pure

Table IV
Reduced Young's modulus (E_r, GPa).

	Ni (US)	Ni-SiC (US)	Ni-MoS_2 (US)	Ni-Mix (US)
Er (GPa)	170.45 ± 5.86	197.32 ± 9.99	178.47 ± 8.62	219.70 ± 18.56

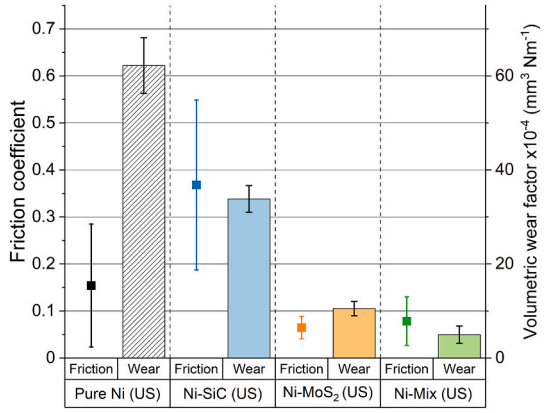

Fig. 7. Average friction coefficient (COF) and volumetric wear factor x10^{-4} (mm^3 Nm^{-1}).

nickel. Many of the physical events during sliding, i.e. ploughing and piling-up of the material, might have increased the average COF. Ni-SiC (US) wear tracks showed (Fig. 8b) flake-like debris with partial detachment, consistent with large adhesive events. Nevertheless, the increase in hardness, as a consequence of both particle hardening and grain size strengthening, halved the worn volume compared to pure Ni (US) (Fig. 7). A similar increase in hardness, accompanied by a decrease in wear, was also reported in previous studies [17,19,40,49] of SiC-based nickel nanocomposites.

Ni-MoS$_2$(US) and Ni-Mix(US) showed low COF (≈0.06 and ≈0.07) compared to pure Ni(US) due to the self-lubrication capability provided by MoS$_2$. Several studies [15,16,30,31,48] have reported a similar decreased in friction by adding MoS$_2$ to Ni coatings. The easy shearing provided by the weak interlayer bonds (van der Waals) in MoS$_2$ [16] was critical to allow self-lubrication and avoid ploughing. Thus, providing a smooth sliding resulting in no debris in the wear tracks or piling-up (Fig. 8c and d). As the result of the combined effect of self-lubrication and high hardness, wear was significantly decreased.

The synergies of combining SiC and MoS$_2$ as particles mixture were visible in the Ni-Mix(US) as the wear factor value was the lowest among the composites. Provided with self-lubrication by MoS$_2$ and high hardness due to nanocrystallinity and significant SiC incorporation, the volumetric wear factor of the deposits was almost 12 times lower than pure Ni(US) (Fig. 7) and with a nearly visible wear track with no pile-up (Fig. 8d). Previous studies with mixed PTFE:SiC [22,43], or mixed WC:WS$_2$ [30] reported similar results where designed as mixed dispersions, lubricant particles combined with hard carbides improved the wear resistance of Ni-based composites, outperforming single particles composites.

4. Conclusions

Ultrasonic agitation was employed to prevent porosity and dendritic growth in the deposits as the result of the agglomeration of conductive MoS$_2$ particles. In order to address the loss of process current efficiency due to the combined effect of ultrasounds and MoS$_2$ particles, the electrodeposition was optimised by adjusting the current density. This combined effect should be further investigated by current transient studies of the kinetics of nucleation and growth of nickel electrocrystallisation under dynamic control of ultrasound.

The combined effect of hardening by SiC incorporation and the resulting grain refinement due to particles codeposition caused strengthening in these deposits, showing higher hardness values (≈448 HV) than pure Ni(US) deposits (≈270 HV). The increase of hardness led to a reduction in the volumetric wear rate in Ni-SiC(US), halving the values reported in pure Ni(US). The incorporation of MoS$_2$ particles caused a higher grain refinement than SiC, provoking nanocrystallinity in the nickel matrix. Thanks to the finer microstructure, Ni-MoS$_2$(US) microhardness (≈446 HV) was comparable to Ni-SiC(US), despite the softening effect of the softer MoS$_2$ particles. The particles also provided self-lubrication to the deposits, reducing the friction coefficient from ≈0.15 in pure Ni to ≈0.06. The combined effect of smooth sliding and high hardness resulted in decreased wear rate (≈5 × 10^{-4} mm^3 Nm^{-1}) compared to Ni(US) (≈62 × 10^{-4} mm^3 Nm^{-1}) and Ni-SiC(US) (≈34 × 10^{-4} mm^3 Nm^{-1}).

Ni-Mix(US) deposits showed all the combined benefits observed individually in the single powder composites. The deposit showed

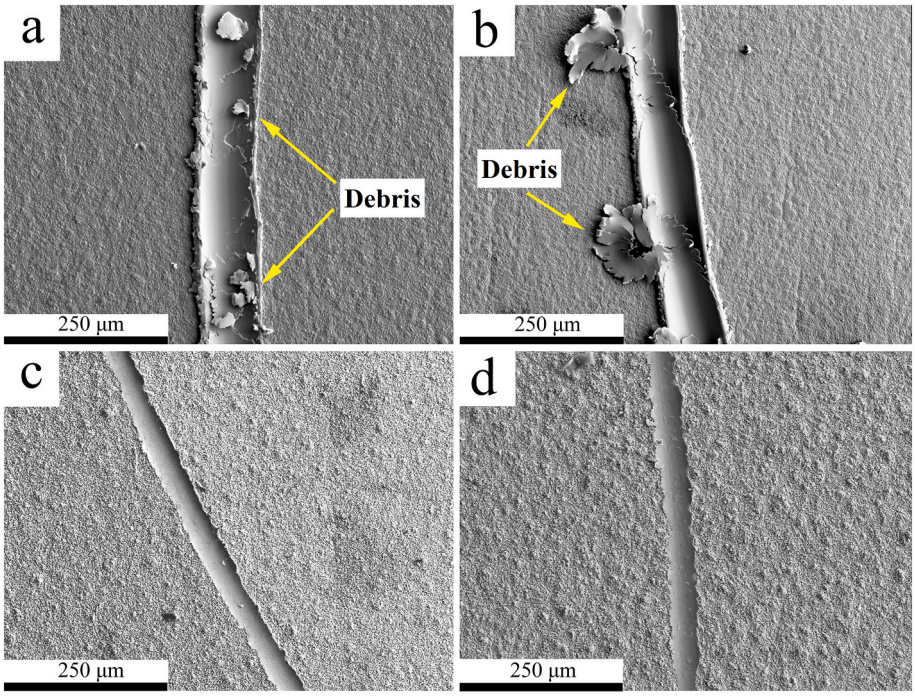

Fig. 8. SE image of the wear tracks (a) Pure Ni US/DC4 (b) Ni-SiC US/DC4 (c) Ni-MoS$_2$ US/DC4 (d) Ni-Mix US/DC2.3.

extremely high hardness values (≈1110 HV) resulting from the significant SiC incorporation (≈15 vol%) and the resulting nanocrystalline structures due to MoS_2 codeposition, in addition to self-lubrication capability. The combined effect of the high hardness and low friction coefficients (≈0.08) limited the effect of the counter material, showing only a nearly visible wear track with no pile-up and a reduced volumetric wear factor, more than 12 times smaller than pure Ni.

CRediT authorship contribution statement

S. Pinate: Conceptualization, Methodology, Validation, Formal analysis, Investigation, Writing – original draft, Visualization. **P. Leisner:** Methodology, Validation, Writing – review & editing. **C. Zanella:** Conceptualization, Methodology, Validation, Formal analysis, Resources, Writing – review & editing, Visualization, Supervision, Project administration, Funding acquisition.

Declaration of competing interest

The authors declare that they have no known competing financial interests or personal relationships that could have appeared to influence the work reported in this paper.

Acknowledgement

The research was partially funded by the project FunDisCo (project reference number 20310117) supported by the Stiftelsen för Kunskaps- och Kompetensutveckling, Sweden, that is kindly acknowledged. Prof. Per Persson and Dr. Ingemar Persson, Linköping University, Sweden, are gratefully acknowledged for performing the TEM imaging and analysis.

References

[1] C. Kerr, D. Barker, F. Walsh, J. Archer, The electrodeposition of composite coatings based on metal matrix-included particle deposits, Trans. IMF 78 (2000) 171–178, https://doi.org/10.1080/00202967.2000.11871333.
[2] A. Leyland, A. Matthews, On the significance of the H/E ratio in wear control: a nanocomposite coating approach to optimised tribological behaviour, Wear 246 (2000) 1–11, https://doi.org/10.1016/S0043-1648(00)00488-9.
[3] Z. Mahidashti, M. Aliofkhazraei, N. Lotfi, Review of nickel-based electrodeposited tribo-coatings, Trans. Indian Inst. Metals 71 (2018) 257–295, https://doi.org/10.1007/s12666-017-1175-x.
[4] S. Wang, C. Ma, F.C. Walsh, Alternative tribological coatings to electrodeposited hard chromium: a critical review, Transactions of the IMF 98 (2020) 173–185, https://doi.org/10.1080/00202967.2020.1776962.
[5] E.A. Pavlatou, M. Stroumbouli, P. Gyftou, N. Spyrellis, Hardening effect induced by incorporation of SiC particles in nickel electrodeposits, J. Appl. Electrochem. 36 (2006) 385–394, https://doi.org/10.1007/s10800-005-9082-y.
[6] S. Pinate, P. Leisner, C. Zanella, Electrocodeposition of nano-SiC particles by pulse-reverse under an adapted waveform, J. Electrochem. Soc. 166 (2019) D804–D809, https://doi.org/10.1149/2.0441915jes.
[7] M.R. Vaezi, S.K. Sadrnezhaad, L. Nikzad, Electrodeposition of Ni–SiC nano-composite coatings and evaluation of wear and corrosion resistance and electroplating characteristics, Colloids Surf. A Physicochem. Eng. Asp. 315 (2008) 176–182, https://doi.org/10.1016/j.colsurfa.2007.07.027.
[8] K. Hou, M. Ger, L. Wang, S. Ke, The wear behaviour of electro-codeposited Ni–SiC composites, Wear 253 (2002) 994–1003, https://doi.org/10.1016/S0043-1648(02)00222-3.
[9] I. Tudela, Y. Zhang, M. Pal, I. Kerr, A.J. Cobley, Ultrasound-assisted electrodeposition of composite coatings with particles, Surf. Coat. Technol. 259 (2014) 363–373, https://doi.org/10.1016/j.surfcoat.2014.06.023.
[10] L. Benea, E. Danaila, J.-P. Celis, Influence of electro-co-deposition parameters on nano-TiO_2 inclusion into nickel matrix and properties characterization of nanocomposite coatings obtained, Mater. Sci. Eng. A 610 (2014) 106–115, https://doi.org/10.1016/j.msea.2014.05.028.
[11] H. Gül, F. Kılıç, S. Aslan, A. Alp, H. Akbulut, Characteristics of electro-co-deposited Ni–Al_2O_3 nano-particle reinforced metal matrix composite (MMC) coatings, Wear 267 (2009) 976–990, https://doi.org/10.1016/j.wear.2008.12.022.
[12] T. Lampke, A. Leopold, D. Dietrich, G. Alisch, B. Wielage, Correlation between structure and corrosion behaviour of nickel dispersion coatings containing ceramic particles of different sizes, Surf. Coat. Technol. 201 (2006) 3510–3517, https://doi.org/10.1016/j.surfcoat.2006.08.073.
[13] V. Medeliene, The influence of B_4C and SiC additions on the morphological, physical, chemical and corrosion properties of Ni coatings, Surf. Coat. Technol. 154 (2002) 104–111, https://doi.org/10.1016/S0257-8972(01)01703-0.
[14] Y. He, W.T. Sun, S.C. Wang, P. Reed, F.C. Walsh, An electrodeposited Ni-P-WS_2 coating with combined super-hydrophobicity and self-lubricating properties, Electrochim. Acta 245 (2017) 872–882, https://doi.org/10.1016/j.electacta.2017.05.166.
[15] M.F. Cardinal, P.A. Castro, J. Baxi, H. Liang, F.J. Williams, Characterization and frictional behavior of nanostructured Ni–W–MoS_2 composite coatings, Surf. Coat. Technol. 204 (2009) 85–90, https://doi.org/10.1016/j.surfcoat.2009.06.037.
[16] Y. He, S.C. Wang, F.C. Walsh, Y.-L. Chiu, P. Reed, Self-lubricating Ni-P-MoS_2 composite coatings, Surf. Coat. Technol. 307 (2016) 926–934, https://doi.org/10.1016/j.surfcoat.2016.09.078.
[17] A. Lanzutti, M. Lekka, C. de Leitenburg, L. Fedrizzi, Effect of pulse current on wear behavior of Ni matrix micro-and nano-SiC composite coatings at room and elevated temperature, Tribol. Int. 132 (2019) 50–61, https://doi.org/10.1016/j.triboint.2018.12.011.
[18] H. Gül, F. Kılıç, M. Uysal, S. Aslan, A. Alp, H. Akbulut, Effect of particle concentration on the structure and tribological properties of submicron particle SiC reinforced Ni metal matrix composite (MMC) coatings produced by electrodeposition, Appl. Surf. Sci. 258 (2012) 4260–4267, https://doi.org/10.1016/j.apsusc.2011.12.069.
[19] Y. Zhou, H. Zhang, B. Qian, Friction and wear properties of the co-deposited Ni–SiC nanocomposite coating, Appl. Surf. Sci. 253 (2007) 8335–8339, https://doi.org/10.1016/j.apsusc.2007.04.047.
[20] F.C. Walsh, S. Wang, N. Zhou, The electrodeposition of composite coatings: diversity, applications and challenges, Curr. Opin. Electrochem. 20 (2020) 8–19, https://doi.org/10.1016/j.coelec.2020.01.011.
[21] S. Pinate, C. Zanella, Wear behavior of Ni-based composite coatings with dual nano-SiC: graphite powder mix, Coatings 10 (2020) 1060, https://doi.org/10.3390/coatings10111060.
[22] Y.S. Huang, X.T. Zeng, I. Annergren, F.M. Liu, Development of electroless NiP–PTFE–SiC composite coating, Surf. Coat. Technol. 167 (2003) 207–211, https://doi.org/10.1016/S0257-8972(02)00899-X.
[23] A. Tang, M. Wang, W. Huang, X. Wang, Composition design of Ni–nano-Al_2O_3–PTFE coatings and their tribological characteristics, Surf. Coat. Technol. 282 (2015) 121–128, https://doi.org/10.1016/j.surfcoat.2015.10.034.
[24] J. Zhou, G. Zhao, J. Li, J. Chen, S. Zhang, J. Wang, F.C. Walsh, S. Wang, Y. Xue, Electroplating of non-fluorinated superhydrophobic Ni/WC/WS_2 composite coatings with high abrasive resistance, Appl. Surf. Sci. 487 (2019) 1329–1340, https://doi.org/10.1016/j.apsusc.2019.05.244.
[25] O.P. Watts, Rapid nickel plating, Trans. Am. Electrochem. Soc. 29 (1916) 395–403.
[26] J. Macheras, D. Vouros, C. Kollia, N. Spyrellis, Nickel electrocrystallization: influence of unsaturated organic additives on the mechanism of the oriented crystal growth, Trans. Inst. Met. Finish. 74 (2) (1996).
[27] Y. Nakamura, N. Kaneko, M. Watanabe, H. Nezu, Effects of saccharin and aliphatic alcohols on the electrocrystallization of nickel, J. Appl. Electrochem. 24 (1994) 227–232, https://doi.org/10.1007/BF00242888.
[28] R. Vittal, H. Gomathi, K.-J. Kim, Beneficial role of surfactants in electrochemistry and in the modification of electrodes, Adv. Colloid Interface Sci. 119 (2006) 55–68, https://doi.org/10.1016/j.cis.2005.09.004.
[29] F.C. Walsh, C.T.J. Low, J.O. Bello, Influence of surfactants on electrodeposition of a Ni-nanoparticulate SiC composite coating, Transactions of the IMF 93 (2015) 147–156, https://doi.org/10.1179/0020296715Z.000000000237.
[30] N. Zhou, S. Wang, F.C. Walsh, Effective particle dispersion via high-shear mixing of the electrolyte for electroplating a nickel-molybdenum disulphide composite, Electrochim. Acta 283 (2018) 568–577. https://doi.org/10.1016/j.electacta.2018.06.187.
[31] Z. Huang, D. Xiong, MoS_2 coated with Al_2O_3 for Ni–MoS_2/Al_2O_3 composite coatings by pulse electrodeposition, Surf. Coat. Technol. 202 (2008) 3208–3214, https://doi.org/10.1016/j.surfcoat.2007.11.033.
[32] G. Li, Q. Qiao Du Zhang, Y. Yu, D. Peterson, A. Zafar, R. Kumar, S. Curtarolo, F. Hunte, S. Shannon, Y. Zhu, W. Yang, L. Cao, All the catalytic active sites of MoS2 for hydrogen evolution, J. Am. Chem. Soc. 138 (2016) 16632–16638, https://doi.org/10.1021/jacs.6b05940.
[33] C. Zanella, M. Lekka, P.L. Bonora, Effect of ultrasound vibration during electrodeposition of Ni–SiC nanocomposite coatings, Surf. Eng. 26 (2013) 511–518. https://doi.org/10.1179/174329409X438961.
[34] I. Tudela, Y. Zhang, M. Pal, I. Kerr, A.J. Cobley, Ultrasound-assisted electrodeposition of thin nickel-based composite coatings with lubricant particles, Surf. Coat. Technol. 276 (2015) 89–105, https://doi.org/10.1016/j.surfcoat.2015.06.030.
[35] E. García-Lecina, I. García-Urrutia, J.A. Díez, J. Fornell, E. Pellicer, J. Sort, Codeposition of inorganic fullerene-like WS_2 nanoparticles in an electrodeposited nickel matrix under the influence of ultrasonic agitation, Electrochim. Acta 114 (2013) 859–867, https://doi.org/10.1016/j.electacta.2013.04.088.
[36] Y.-C. Chang, Y.-Y. Chang, C.-I. Lin, Process aspects of the electrolytic codeposition of molybdenum disulfide with nickel, Electrochim. Acta 43 (1998) 315–324, https://doi.org/10.1016/S0013-4686(97)00072-8.
[37] J. Amblard, I. Epelboin, M. Froment, G. Maurin, Inhibition and nickel electrocrystallization, J. Appl. Electrochem. 9 (1979) 233–242, https://doi.org/10.1007/BF00616093.
[38] S. Coleman, S. Roy, Effect of ultrasound on mass transfer during electrodeposition for electrodes separated by a narrow gap, Chem. Eng. Sci. 113 (2014) 35–44, https://doi.org/10.1016/j.ces.2014.03.026.
[39] P. Gyftou, E.A. Pavlatou, N. Spyrellis, Effect of pulse electrodeposition parameters on the properties of Ni/nano-SiC composites, Appl. Surf. Sci. 254 (2008) 5910–5916, https://doi.org/10.1016/j.apsusc.2008.03.151.

[40] P. Gyftou, M. Stroumbouli, E.A. Pavlatou, P. Asimidis, N. Spyrellis, Tribological study of Ni matrix composite coatings containing nano and micro SiC particles, Electrochim. Acta 50 (2005) 4544–4550, https://doi.org/10.1016/j.electacta.2004.10.090.
[41] T. Lampke, B. Wielage, D. Dietrich, A. Leopold, Details of crystalline growth in co-deposited electroplated nickel films with hard (nano)particles, Appl. Surf. Sci. 253 (2006) 2399–2408, https://doi.org/10.1016/j.apsusc.2006.04.060.
[42] S. Pinate, A. Ispas, P. Leisner, C. Zanella, Electrocodeposition of Ni composites and surface treatment of SiC nano-particles, Surf. Coat. Technol. 406 (2021) 126663, https://doi.org/10.1016/j.surfcoat.2020.126663.
[43] W. Jiang, L. Shen, Z. Wang, K. Wang, M. Xu, Z. Tian, Wear resistance of a Ni-PTFE composite coating strengthened with nano-SiC particles, Mater. Res. Express 6 (2019) 96443, https://doi.org/10.1088/2053-1591/ab320b.
[44] E. García-Lecina, I. García-Urrutia, J.A. Díez, J. Morgiel, P. Indyka, A comparative study of the effect of mechanical and ultrasound agitation on the properties of electrodeposited Ni/Al_2O_3 nanocomposite coatings, Surf. Coat. Technol. 206 (2012) 2998–3005, https://doi.org/10.1016/j.surfcoat.2011.12.037.
[45] I. Tudela, Y. Zhang, M. Pal, I. Kerr, T.J. Mason, A.J. Cobley, Ultrasound-assisted electrodeposition of nickel: effect of ultrasonic power on the characteristics of thin coatings, Surf. Coat. Technol. 264 (2015) 49–59, https://doi.org/10.1016/j.surfcoat.2015.01.020.
[46] Z. Li, J. Wang, J. Lu, J. Meng, Tribological characteristics of electroless Ni–P–MoS_2 composite coatings at elevated temperatures, Appl. Surf. Sci. 264 (2013) 516–521, https://doi.org/10.1016/j.apsusc.2012.10.055.
[47] C. Zanella, M. Lekka, P.L. Bonora, Influence of the particle size on the mechanical and electrochemical behaviour of micro- and nano-nickel matrix composite coatings, J. Appl. Electrochem. 39 (2009) 31–38, https://doi.org/10.1007/s10800-008-9635-y.
[48] S.M.J.S. Shourije, M.E. Bahrololoom, Effect of current density, MoS_2 content and bath agitation on tribological properties of electrodeposited nanostructured Ni-MoS_2 composite coatings, Tribol.-Mater. Surf. Interf. 13 (2019) 76–87, https://doi.org/10.1080/17515831.2019.1589160.
[49] G. Gyawali, B. Joshi, K. Tripathi, S.W. Lee, Effect of ultrasonic nanocrystal surface modification on properties of electrodeposited Ni and Ni-SiC composite coatings, J. Mater. Eng. Perform. 26 (2017) 4462–4469, https://doi.org/10.1007/s11665-017-2891-4.
[50] T. Fritz, M. Griepentrog, W. Mokwa, U. Schnakenberg, Determination of Young's modulus of electroplated nickel, Electrochim. Acta 48 (2003) 3029–3035, https://doi.org/10.1016/S0013-4686(03)00370-0.
[51] M.F. Ashby, Materials Selection in Mechanical Design, fourth edition, Elsevier/Butterworth-Heinemann, Amsterdam, 2011.
[52] G. Magnani, S. Galvagno, G. Sico, S. Portofino, C. Freda, E. Burresi, Sintering and mechanical properties of β-SiC powder obtained from waste tires, J. Adv. Ceram. 5 (2016) 40–46, https://doi.org/10.1007/s40145-015-0170-0.
[53] Y. Li, C. Yu, Y. Gan, P. Jiang, J. Yu, Y. Ou, D.-F. Zou, C. Huang, J. Wang, T. Jia, Q. Luo, X.-F. Yu, H. Zhao, C.-F. Gao, J. Li, Mapping the elastic properties of two-dimensional MoS_2 via bimodal atomic force microscopy and finite element simulation, npj Comput. Mater. 4 (2018) 49, https://doi.org/10.1038/s41524-018-0105-8.
[54] C. Donnet, A. Erdemir, Historical developments and new trends in tribological and solid lubricant coatings, Surf. Coat. Technol. 180–181 (2004) 76–84, https://doi.org/10.1016/j.surfcoat.2003.10.022.
[55] I. Hutchings, P. Shipway, Tribology: Friction and Wear of Engineering Materials, second edition, Elsevier / Butterworth-Heinemann, Amsterdam, 2017.
[56] K. Holmberg, H. Ronkainen, A. Laukkanen, K. Wallin, Friction and wear of coated surfaces — scales, modelling and simulation of tribomechanisms, Surf. Coat. Technol. 202 (2007) 1034–1049, https://doi.org/10.1016/j.surfcoat.2007.07.105.
[57] L. Benea, P.L. Bonora, A. Borello, S. Martelli, Wear corrosion properties of nano-structured SiC–nickel composite coatings obtained by electroplating, Wear 249 (2002) 995–1003, https://doi.org/10.1016/S0043-1648(01)00844-4.